

Sudden collapse

Shells are very efficient in carrying load. However, this efficiency comes at a price. If a shell buckles, it collapses with a bang. There will be no warning and it will collapse faster than we can run.

Truss, frame and plate structures do not have this problem. Usually, they slowly deform a lot before collapsing and therefore they give clear warnings to evacuate the area.

Consequently, shells need to be extra safe. In other words, for shells we often use larger load factors and material factors than for most structures. In the eurocode this is organised in consequence classes. Often, the highest consequence class is appropriate.

Tucker High School

On September 14, 1970, the gymnasium of The Tucker High School in, Henrico County, Virginia, collapsed completely [81]. Some school children were injured but fortunately there was no loss of life. The structure was a four element [hypar](#) (p. 117) with a plan of 47.2 m by 49.4 m (fig. 180). It had a [sagitta](#) (p. 1) of about 4.6 m, large inclined supporting ribs and centre ribs that were essentially concentric with the shell. The shell was 90 mm thick for the most part. Therefore, it had a ratio $\frac{a}{t} = \frac{47.2/2 \times 49.4/2}{4.6 \times 0.090} = 1400$.

The failure was due to progressive deflection. The lightweight concrete showed much creep. Three similar structures were subsequently demolished. One of these had a deflection of 460 mm at the centre. Research showed that the collapse could have been simply prevented by cambering upward the centre point of the shell [81].



ipped roof gymnasium was one of four identical structures designed by same firm.



Figure 180. Newspaper photograph of the collapsed hypar shell [81]

Cylinder buckling shapes

The buckling shape of an axially loaded cylinder can start as ring mode or a chess board mode (fig. 181). Which one occurs depends on the shell thickness and its radius. When buckling progresses the ring mode can transform into the chess board mode. However, these deformations are very small and rarely visible. When the material starts to deform plastically the ring mode develops into an elephant foot (fig. 182); the chess board mode develops into a Yoshimura¹ pattern (fig. 183), which are clearly visible.

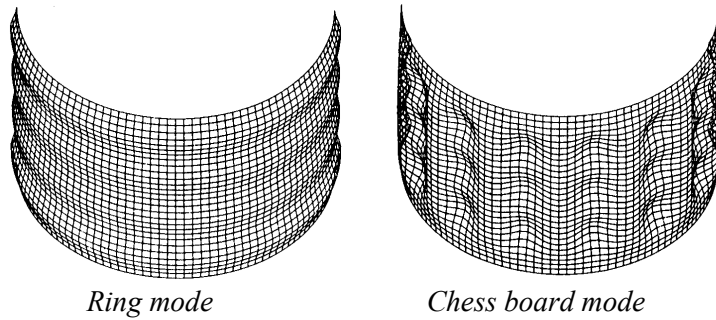


Figure 181. Buckling modes of axially compressed cylinders computed by the finite element method (The deformation is enlarged to make it visible.)

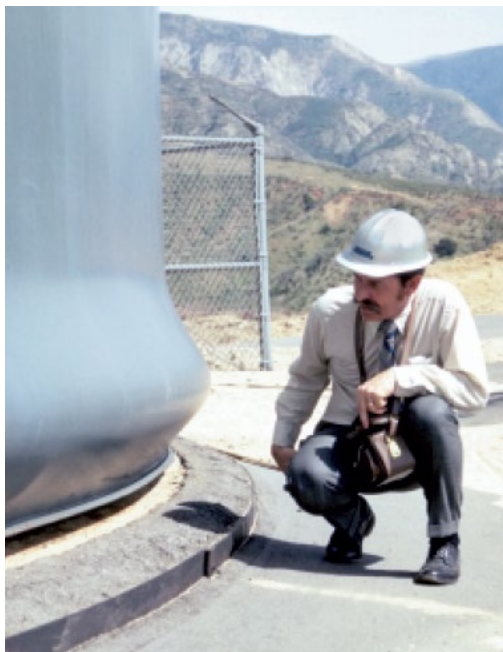


Figure 182. Elephant foot buckling of a tank wall [82]



Figure 183. Yoshimura buckling of an aluminium cylinder

Exercise: The Yoshimura pattern can be obtained as an origami exercise. Take a sheet of paper and draw the lines of figure 184 on it. Fold all horizontal lines towards you and all diagonal lines away from you. When all folds are made the sheet tends to curve. Curve the sheet further and close it with sticky tape.

¹ Yoshimura Yoshimaru (吉村 慶丸) (approximately 1920-1964) was a professor of applied mechanics at Tokyo University of Technology. Nine years after the Second World War, he was invited to the USA to work on shell structures. There, he wrote a report [83] which explained the buckling shape that was often observed in cylinder experiments. Unfortunately for many of us, his other publications are in Japanese.

Remarkable about the Yoshimura pattern is that it is *inextensional* (p. 109). Fortunately, large extensions are needed to transform a cylinder directly into a Yoshimura pattern [83]. You can try this too: Take a sheet of paper, curve it into a cylinder and close it with sticky tape. Then load the cylinder axially by books until it buckles. If the cylinder and the load are nearly perfect, then the cylinder deforms into a Yoshimura pattern. Clearly, reality is not perfect. Nevertheless, several Yoshimura buckles can be recognised in the overloaded cylinder.

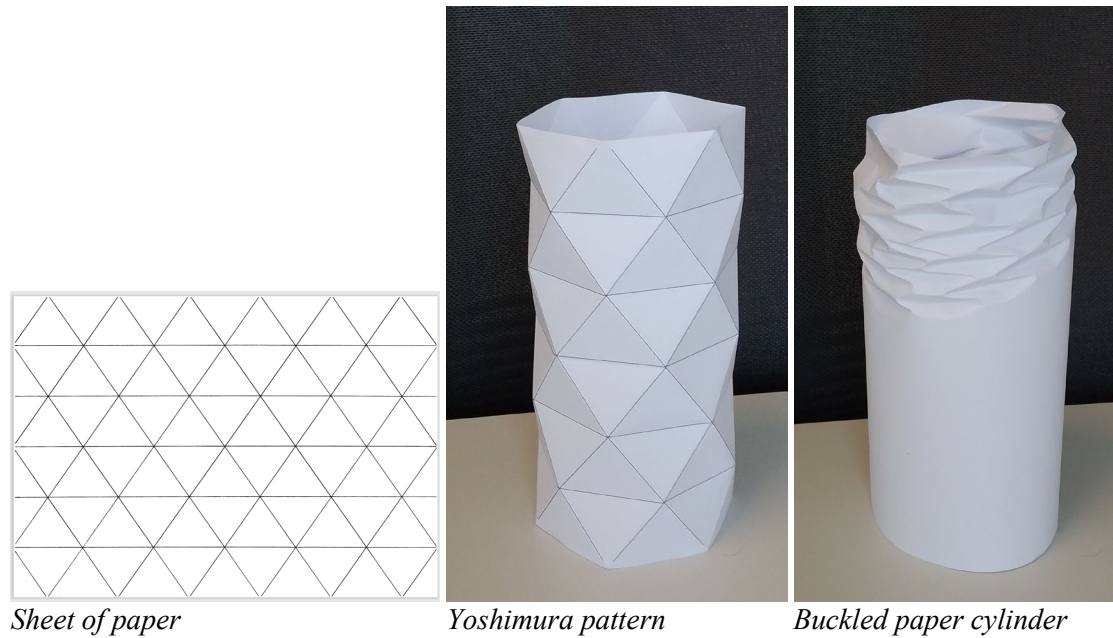


Figure 184. Origami exercise

Buckling of a beam supported by springs

Shells can be understood by studying a beam supported by uniformly distributed springs (fig. 185). The bending stiffness of the beam is EI [Nm²]. The stiffness of the distributed springs is k [N/m²]. The beam is loaded by an axial force P [kN]. The differential equation that describes this beam is

$$EI \frac{d^4 w}{dx^4} + P \frac{d^2 w}{dx^2} + k w = 0.$$

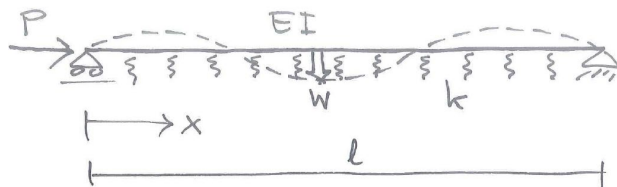


Figure 185. Elastic beam supported by distributed springs

The following buckling shape is proposed

$$w = b \sin \frac{n\pi x}{l},$$

where n is the number of half waves of the buckled shape. Substitution of the buckling shape into the differential equation gives the following solution.

```
> w:=b*sin(n*Pi*x/l):
> eq:=EI*diff(w,x,x,x,x)+P*diff(w,x,x)+k*w=0:
> Pcr:=expand(solve(eq,P));
```

$$P_{cr} = \frac{n^2 \pi^2 EI}{l^2} + \frac{kl^2}{n^2 \pi^2}$$

This solution is plotted in figure 186 in dimension less quantities. It shows that for long beams the red line is a good approximation.

$$P_{cr} \approx 2\sqrt{kEI}.$$

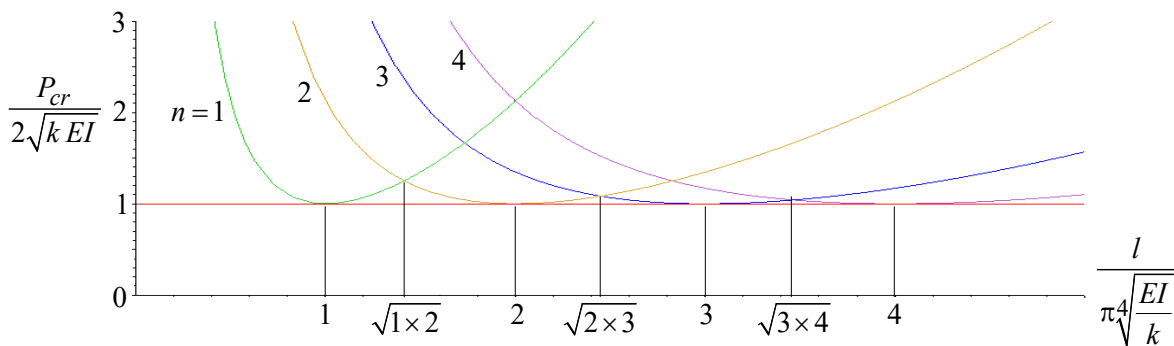


Figure 186. Buckling load as a function of the beam length

Ring buckling of an axially compressed cylinder

Consider a circular cylinder (fig. 187).

$$k_{xx} = 0, \quad k_{yy} = \frac{1}{a}, \quad k_{xy} = 0, \quad \alpha_x = \alpha_y = 1, \quad 0 \leq u \leq l, \quad 0 \leq v \leq 2\pi a$$

Somebody proposes the following deformation.

$$u_x = \frac{v}{a} \int w(u) du, \quad u_y = 0, \quad u_z = w(u).$$

This deformation is axial symmetric and depends on an unknown function w . Please note the difference between ν (Poisson's ratio) and v (curvilinear coordinate).

Substitution in the 21 Sanders-Koiter equations (p. 54) gives

$$\frac{Et^3}{12(1-\nu^2)} \frac{d^4 w}{dx^4} + \frac{Et}{a^2} w = n_{xx} \frac{d^2 w}{dx^2}.$$

This is the same differential equation as that of buckling of a beam supported by springs (p. 137). Apparently we can make the following interpretations.

$$\frac{Et^3}{12(1-\nu^2)} = EI, \quad \frac{Et}{a^2} = k, \quad n_{xx} = -P$$

Using this analogy, the buckling load of a not short cylinder is calculated as

$$n_{cr} = -2\sqrt{kEI} = \frac{-1}{\sqrt{3(1-\nu^2)}} \frac{Et^2}{a} \quad \boxed{n_{cr} \approx -0.6 \frac{Et^2}{a}}$$

and the buckling length is

$$l_{cr} = \pi^4 \sqrt[4]{\frac{EI}{k}} = \frac{\pi\sqrt{at}}{\sqrt[4]{12(1-\nu^2)}} \approx 1.7\sqrt{at}.$$

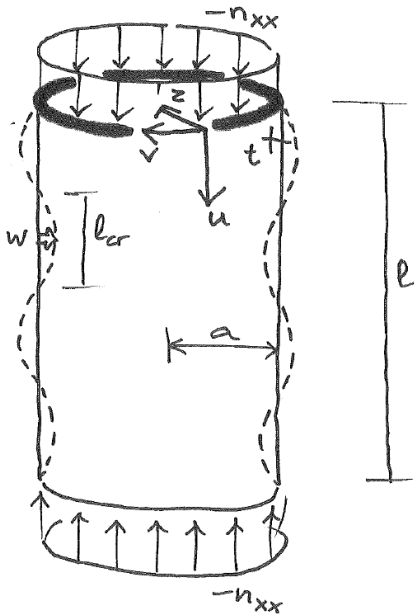


Figure 187. Cylinder coordinate system

Exercise: Calculate the buckling length of a cylinder made out of a sheet of paper.

Exercise: In what shape does a very long cylinder buckle?

Exercise: What is the difference between the buckling length and the [influence length](#) (p. 73)?

Differential equation for shell buckling

The differential equation for shell buckling is an extension of the [shallow shell differential equation](#) (p. 59)

$$\frac{Et^3}{12(1-\nu^2)} \nabla^2 \nabla^2 \nabla^2 \nabla^2 u_z + Et \Gamma \Gamma u_z = \nabla^2 \nabla^2 \left(p_z + n_{xx} \frac{\partial^2 u_z}{\partial x^2} + (n_{xy} + n_{yx}) \frac{\partial^2 u_z}{\partial x \partial y} + n_{yy} \frac{\partial^2 u_z}{\partial y^2} \right)$$

It can be easily derived starting with [Sanders-Koiter equation 21](#) (p. 54) by replacing k_{xx} by

$k_{xx} + \frac{\partial^2 u_z}{\partial x^2}$ et cetera. This differential equation can be solved analytically for elementary

shell shapes and elementary loading. The buckling loads thus obtained are called *critical loads*. There is a large body of literature on this. Scientists who made significant contributions are Rudolf Lorenz, Stephen Timoshenko, Richard Southwell, Richard von Mises, Wilhelm Flügge, Lloyd Donnell. An overview is given by Nicholas Hoff [84] ².

Buckling load factor

A load factor λ is introduced in the [differential equation for shell buckling](#) (p. 139).

$$\frac{Et^3}{12(1-\nu^2)} \nabla^2 \nabla^2 \nabla^2 \nabla^2 u_z + Et \Gamma \Gamma u_z = \nabla^2 \nabla^2 (\lambda p_z + \lambda n_{xx} \frac{\partial^2 u_z}{\partial x^2} + \lambda (n_{xy} + n_{yx}) \frac{\partial^2 u_z}{\partial x \partial y} + \lambda n_{yy} \frac{\partial^2 u_z}{\partial y^2})$$

A chess board buckling pattern is assumed.

$$u_z = c \cos \frac{\pi x}{l_x} \cos \frac{\pi y}{l_y}$$

The following assumptions simplify the mathematics.

$n_{xy} + n_{yx} = 0$... the buckles occur in the principal membrane force directions,

$k_{xy} = 0$ the buckles occur in the principal curvature directions.

The buckling pattern and the assumptions are substituted in the differential equation and the critical load factor is solved (appendix 10).

$$\lambda_{cr} = \frac{-Et}{\frac{n_{xx}}{l_x^2} + \frac{n_{yy}}{l_y^2}} \left(\frac{\pi^2 t^2}{12(1-\nu^2)} \left(\frac{1}{l_x^2} + \frac{1}{l_y^2} \right)^2 + \frac{\left(\frac{k_{xx}}{l_y^2} + \frac{k_{yy}}{l_x^2} \right)^2}{\pi^2 \left(\frac{1}{l_x^2} + \frac{1}{l_y^2} \right)^2} \right)$$

² Stephen Timoshenko (1878-1972) was born in Ukraine and became a professor at Kyiv Polytechnic Institute. In 1919, he fled for the Bolshevik revolution and ended up in the USA where he became a professor at the University of Michigan and later at Stanford University [Wikipedia].

Richard von Mises (1883-1953) was born in Ukraine. He studied at Vienna University of Technology. He was a pilot during the First World War and afterwards a professor of applied mathematics in Dresden and Berlin. He was Jewish and in 1933 he left nazi Germany to teach in Istanbul. Later he moved to Harvard University, USA [Wikipedia].

Rudolf Lorenz (18...-19...) was a civil engineer in Dortmund, Germany [84].

Richard Southwell (1888-1970) was a mathematician and engineer. He taught at the University of Cambridge, Oxford and Imperial College London [Wikipedia].

Lloyd Donnell (1895-1997) was an American engineer, professor at Illinois Institute of Technology and Stanford University [Wikipedia].

Wilhelm Flügge (1904-1990) was a German engineer. After the second world war he moved to the USA and became professor at Stanford University [German Wikipedia].

Nicholas Hoff (1906-1997) was born in Hungary. He studied aeronautical engineering at Stanford University before the war and eventually became a professor there. He was a student of Timoshenko [Wikipedia].

Suppose that buckling is not restrained by edges, then the buckling lengths l_x and l_y are such that the load factor is smallest. This was studied by plotting λ_{cr} as function of l_x and l_y for various values of $n_{xx}, n_{yy}, k_{xx}, k_{yy}$ (appendix 10). The result is surprisingly simple. Three buckling modes can occur.

$$\lambda_{cr1} = \frac{-Et^2}{\sqrt{3(1-\nu^2)}} \frac{|k_{yy}|}{n_{xx}} \quad \lambda_{cr2} = \frac{-Et^2}{\sqrt{3(1-\nu^2)}} \frac{|k_{xx}|}{n_{yy}} \quad \lambda_{cr3} \approx 0$$

The third buckling mode is due to inextensional deformation. Sometimes these buckling load factors are negative, which shows that we need to reverse the load to cause buckling.

Exercise: Are the formulas for cylinder ring buckling and cylinder chess board buckling the same?

Exercise: What is the buckling formula for a spherical shell loaded by a vacuum?

Challenge: The numerical study seems to show that

$$\lambda_{cr3} < 0 \quad \text{for} \quad n_{xx}|k_{xx}| + n_{yy}|k_{yy}| > 0 \quad (\text{not dangerous})$$

$$\lambda_{cr3} = \infty \quad \text{for} \quad n_{xx}|k_{xx}| + n_{yy}|k_{yy}| = 0 \quad (\text{not dangerous})$$

$$\lambda_{cr3} > 0 \quad \text{for} \quad n_{xx}|k_{xx}| + n_{yy}|k_{yy}| < 0 \quad (\text{dangerous}).$$

Prove or disprove this.

Challenge: Derive the buckling formula for $n_{xy} + n_{yx} = 0$ and $k_{xx} = k_{yy} = 0$ and $k_{xy} \neq 0$.

Design check of buckling

For design, the buckling load factors should not be in the interval $0 < \lambda_{cr} < 1$.

This can be explained as follows. Consider a free form shell structure. We specify loads, [safety factors](#) (p. ...) and [load combinations](#) (p. ...). We do a linear analysis to obtain the membrane forces. We do a linear buckling analysis to obtain the buckling load factors for each load combination. Suppose that a buckling load factor is 0.9. This means that when we apply this load combination slowly, the shell will buckle at 90% of the full load. Clearly, this will not do. We need to change the design.

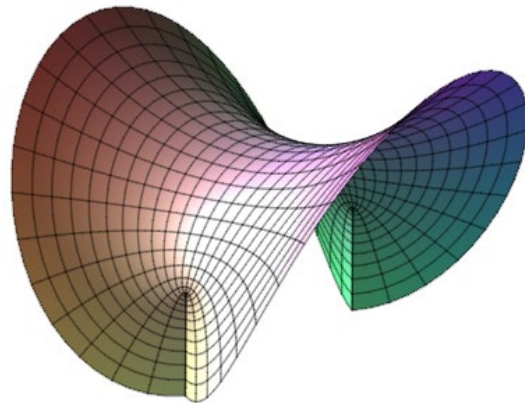
Catelan's surface ³

The Catelan minimal surface is described by the following **orthogonal parameterisation** (p. 25).

$$\bar{x} = au \cos v \quad -1 < u < 1 \quad -\frac{1}{2}\pi < v < \frac{1}{2}\pi$$

$$\bar{y} = \frac{1}{4}a \left((2u^2 + 1) \sin 2v + 2v \right)$$

$$\bar{z} = \frac{1}{4}a \left((2u^2 + 1) \cos 2v - 1 \right)$$



$$k_{xx} = \frac{\cos v}{a\sqrt{u^2 + 1}(u^2 + \cos^2 v)}$$

$$k_{yy} = -k_{xx}$$

$$k_{xy} = \frac{-u \sin v}{a(u^2 + 1)(u^2 + \cos^2 v)}$$

$$\alpha_x = a\sqrt{u^2 + \cos^2 v}$$

$$\alpha_y = a\sqrt{(u^2 + 1)(u^2 + \cos^2 v)}$$

Imperfection sensitivity

Before 1930, airplanes consisted of frames covered with a fabric which was painted. However, engineers wanted to build airplanes from aluminium plates that were joined to form a cylindrical shape. Therefore, scientists started to do experiments on cylinders, for example Andrew Robertson ⁴. Figure 188 shows the ultimate loads of axially compressed aluminium cylinders. They are much smaller than the critical load. Robertson ends his paper on the subject with “*Further comment as to the insufficiency of these formulae is unnecessary*” [85].

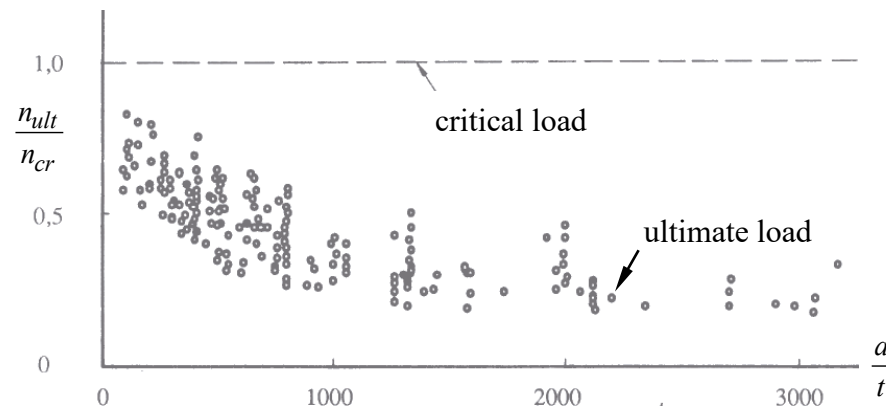


Figure 188. Experimental ultimate loads of 172 axially loaded aluminium cylinders [86]

This difference between theory and experiments is caused by invisible shape imperfections. At first sight, imperfection sensitivity is hard to believe because the experiments were performed very carefully. The aluminium cylinders had perfectly cut edges and were

³ Eugène Catalan (1814 – 1894) was a Belgian mathematician and professor at the University of Liège [Wikipedia].

⁴ Andrew Robertson (1883 – 1977) was a professor of Mechanical Engineering at Bristol University [Wikipedia].

beautifully polished. The cylinders were perfectly centred in the testing machines. The testing machines were modern and very accurate measuring instruments were used. Nonetheless, the ultimate loads were much smaller than the critical loads. Not only compressed cylinders but also bend cylinders and radially compressed domes are very sensitive to shape imperfections.

Experiment

What is the ultimate load of an axially loaded empty beer can? We model the can as an open cylinder. The wall thickness is 0.08 mm the radius is 32.8 mm, Young's modulus is 2.1×10^5 N/mm² and Poisson's ratio is 0.35 (stainless steel). The critical load (p. 139) is



$$n_{cr} = -0.6 \frac{Et^2}{a} = -0.6 \frac{2.1 \times 10^5 \times 0.08^2}{32.8} = -25.3 \text{ N/mm}$$

$$F_{cr} = 2\pi a n_{cr} = 2 \times 3.14 \times 32.8 \times (-25.3) = -5200 \text{ N}$$

Therefore, it should be able to carry a mass of 520 kg pulled by earth's gravity. Carefully stand on the can and it will – probably – carry your weight. Subsequently, use your thumbs to push a dimple in the can and push it out again. Doing so makes typical clicking sounds. Notice that the imperfections you made are hardly visible. Now, try standing on the can again. It will collapse abruptly. The explanation is imperfection sensitivity.

Puzzle

The large difference between the theoretical buckling load (critical load) and the experimental buckling load (ultimate load) puzzled scientists for approximately 10 years. Is the differential equation wrong? Are the solutions to the differential equation wrong? Are there more solutions that we have not found? Is there some mistake in the experimental set up? Has thin aluminium less stiffness than solid aluminium?

The solution was discovered in 1940 by Theodore von Kármán and Qian Xuesen (钱学森 pronounce tsien? sue? sen) [87].⁵ They calculated the load-displacement curve after buckling. Figure 189 shows the result of their calculation; n_{xx} is the membrane force in a cylinder and w is the shortening of the cylinder. Note that load on a perfect cylinder can be increased until the critical load after which the strength will drop strongly. This behaviour is typical for shell structures and very different from other structures. Figure 189b shows that very small shape imperfections cause the ultimate load to be much smaller than the critical load.

⁵ Von Kármán (1881-1963) and Qian (1911-2009) worked at Caltech (California Institute of Technology) as rocket scientists. They developed the knowledge that later showed necessary for the Apollo program (1961-1972), in which USA astronauts walked on the moon. Von Karman was Hungarian and he immigrated to the USA in 1930. Qian was Chinese. He immigrated to the USA in 1935 and back to China in 1955 in not friendly circumstances. The discovery of shell imperfection sensitivity was just a footnote in their lives. More on Von Kármán and on Qian can be found in Wikipedia (Qian's name is often spelled as H.S. Tsien).

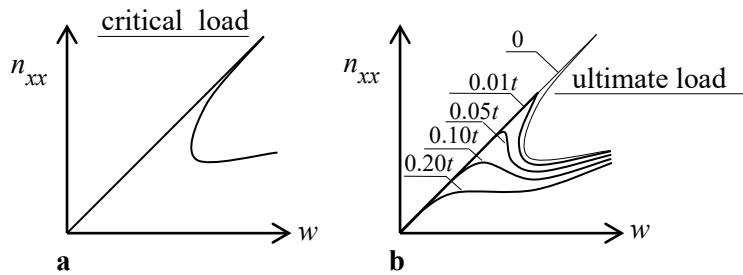


Figure 189. Buckling of cylinders for different shape imperfection amplitudes [87]

Exceptions to imperfection sensitivity

Some shells are not sensitive to imperfections. Radially loaded open cylinders are not because they buckle **inextensionally** (p. 109). Cylinders with torsion loading ($n_{xy} \neq 0$ or $n_{yx} \neq 0$) are not sensitive to imperfections. A **hypar roof** (p. 102) is sensitive to imperfections if it buckles in mode 1 or 2 but not if it buckles in **mode 3** (p. 140).

Koiter's law ⁶

Equilibrium of a perfect system can be described by

$$\lambda = \lambda_{cr} (1 - c_1 w - c_2 w^2),$$

Where λ is the load factor, λ_{cr} is the critical load factor, w is the amplitude of the deflection, c_1 and c_2 are constants characterising the given structure. There are three types of post critical behaviour (fig. 190). Type I behaviour occurs when $c_1 = 0$ and $c_2 < 0$. The structure is not sensitive to imperfections. Type II behaviour occurs when $c_1 = 0$ and $c_2 > 0$. The structure is sensitive to imperfections. Koiter showed that the ultimate load factor is equal to

$$\lambda_{ult} = \lambda_{cr} \left(1 - 3 \left(w_0 \frac{1}{2} \rho \sqrt{c_2} \right)^{\frac{2}{3}} \right),$$

Where ρ is a coefficient depending on the imperfection shape and w_0 is the imperfection amplitude. Type III behaviour occurs when $c_1 > 0$. The structure is very sensitive to imperfections. The ultimate load factor is equal to

$$\lambda_{ult} = \lambda_{cr} \left(1 - 2 \left(w_0 \rho c_1 \right)^{\frac{1}{2}} \right).$$

This is called *Koiter's half power law*.

Properly supported flat plates display type 1 behaviour; They buckle at small normal forces. After buckling the load can be increased substantially. Most thin shells display type III behaviour.

⁶ Warner Koiter (1914-1997) was professor at Delft University of Technology at the faculties of Mechanical Engineering and Aerospace Engineering (1949-1979). He wrote his dissertation during the Second World War, while hiding from Arbeitseinsatz, and published it in 1945 just after the war [88]. The English translation appeared in 1967 [89]. It became famous because it quantifies the imperfection sensitivity of thin shells.

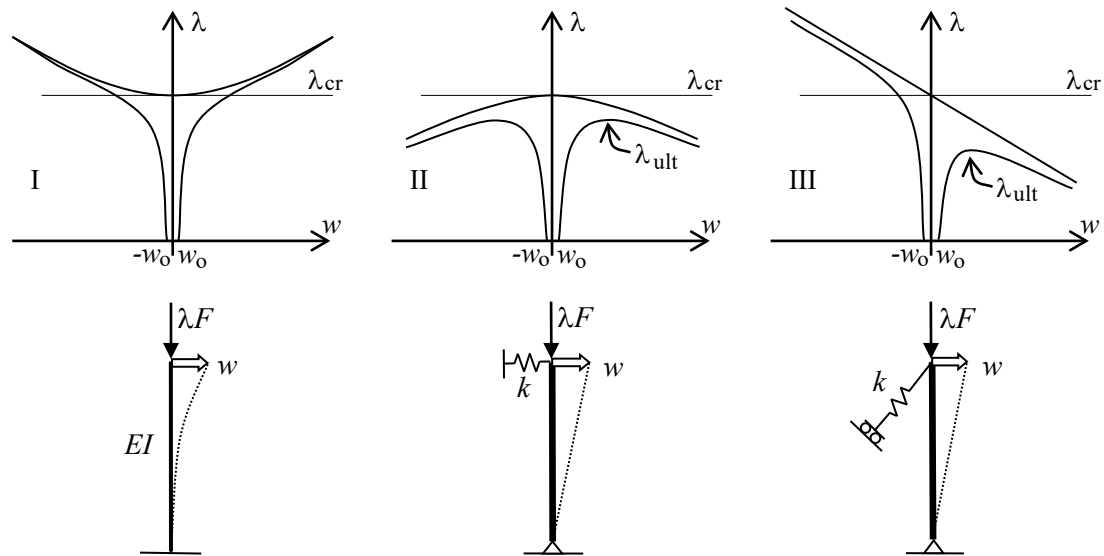


Figure 190. Three types of post buckling behaviour according to Koiter

Knock down factor

In shell design often the following procedure is used. First the critical load is computed by using the formula or a finite element program. Then this loading is reduced by a factor C that accounts for imperfection sensitivity. This factor is called “knock down factor”. The result needs to be larger than the design loading. Often it is determined experimentally. For example, for reinforced concrete sewer pipes loaded in bending the following knock down factor is used.

$$C = 1 - 0.73 \left(1 - e^{-\frac{1}{16} \sqrt{\frac{a}{t}}} \right).$$

The range in which it is valid is $0.5 < \frac{l}{a} < 5$ and $100 < \frac{a}{t} < 3000$ where l is the pipe length [90].

If little information is available the following knock down factor can be used.

$$C = \frac{1}{6}$$

This is based on figure 188 in which all of the tests show an ultimate load more than 0.166 times the critical load.

Linear buckling analysis

Finite element programs can compute critical load factors λ_{cr} and the associated normal modes. This is called a linear buckling analysis. A finite element model has as many critical load factors as the number of degrees of freedom. We can specify how many of the smallest critical load factors the software will compute. If the second smallest buckling load is very close (say within 2%) to the smallest buckling load we can expect the structure to be highly sensitive to imperfections.

Often, the critical load factors need to be multiplied by the knockdown factor. The results need to be larger than 1. Consequently, if all critical load factors are larger than 6, the structure is safe for buckling.

Linear buckling analyses are performed on shell models without imperfections. We could add shape imperfections, however, this would not solve anything. The shape imperfections grow slowly during loading and this is not included in a linear buckling analyses. For imperfections to grow we need to perform a [nonlinear finite element analysis](#) (p. 146).

Ship design

A steel ship consists of plates strengthened by stiffeners. A linear buckling analysis of the ship model produces critical load factors for each plate that buckles. However, flat plates buckle in [Koiter's mode I](#) (p. 144) which does not cause failure. We are interested in buckling of big curved parts of the ship because these go in [Koiter's mode III](#) which does cause failure. A computer cannot tell the difference between plate buckling and shell buckling. The only thing we can do is go through the load factors from small to large, look at each buckling mode and continue until we see buckling that involves more than one plate. This can take much time because a large ship consists of hundreds of plates and has many load combinations.

Oil tanker

In 2000 the oil company Shell had 150 oil tankers in its fleet. In 2019 just 15. The modern oil tankers are more than 300 m long which is much larger than the old ones. (Advantages of large tankers are less fuel cost and fewer collisions because there are fewer ships at sea.) A new oil tanker costs approximately 120 000 000 euro.

Old single hull oil tankers had a single steel shell between the sea and the oil. The tankers were divided in oil tanks. These tanks were sometimes filled with sea water as ballast for levelling the ship. When the ballast water was pumped out the sea was polluted. Also in collisions the sea was polluted. Nowadays, double hull tankers are common. Double hull tankers have two steel shells between the oil and the sea (figure 139). They also have separate tanks for oil and for ballast water. A problem of the double hull tankers is that the ballast tanks corrode. Despite efforts to paint the ballast tanks, the double hull tankers do not last long. The average life time of oil tankers is 10 years.

Figure 139. ... [... p.]

An oil tanker is designed for 20 year. It has three structural limit states: yielding, fatigue and buckling. It has many load cases and about 20 load combinations (table 10).

Current computer capacity is not sufficient to perform a finite element analyses of a tanker in all its details. Therefore, first a rough model is made of the tanker without details. Subsequently, submodels are made of tanker parts. The edges of a submodel are loaded by forces and moments that are automatically transferred from the rough model. This method is called submodelling. For buckling analysis the submodels are much larger than the area of interest because otherwise the free submodel edge would influence the buckling load.

Table 10. Load cases of an oil tanker

Nonlinear finite element analysis

When a shell design is ready it is sensible to check its performance by nonlinear finite element analyses. In these analyses the loading is applied in small increments for which the displacements are computed. Figure 191 shows the results of finite element analyses of a simply supported shallow dome.

The ultimate load is mainly affected by shape imperfections, support stiffness imperfections and yielding or cracking. When these are measured and included in the finite element model, then the predicted ultimate load has a deviation less than 10% of the experimental ultimate load [91].

Clearly, before a shell has been build we cannot measure the imperfections. Instead these are estimated. For example, the amplitude of the geometric imperfections is estimated by the designer and the builder. Often, the analyst will assume that the shape of the geometric imperfections is the first buckling mode. He or she will add this imperfection to the finite element model.

It seems logical that an imperfection shape equal to the buckling shape gives the smallest ultimate load. For columns this is true. However, for shells there exists no mathematical proof of this. Therefore, another imperfection shape might give an even smaller ultimate load [93]. Of course, the analyst can consider only a few imperfection shapes.

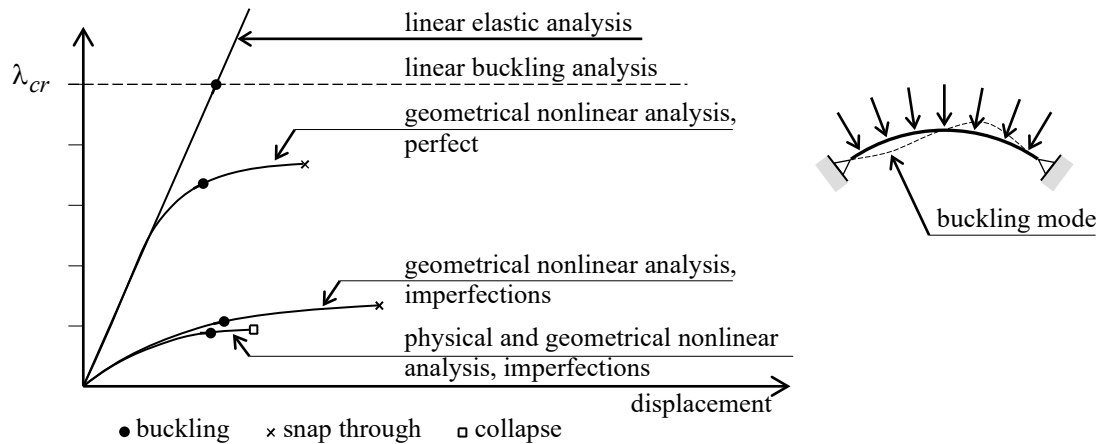


Figure 191. Shell finite element analyses of a steel spherical dome [93]

Mystery solved

The critical and ultimate load of shell structures can be determined by both analytical and numerical analysis. However, these analyses are complicated and many engineers and scientists feel that we still do not understand imperfection sensitivity [94]. Here it is argued that shell buckling is not a mystery at all.

In nonlinear finite element analyses we see that when a small load is applied the shell deforms in a buckling mode. The buckling mode increases the shape imperfections of the shell. The deformation is very small and invisible to the naked eye. Nonetheless, the deformation changes the curvature, in some locations the curvature has become larger and in other locations the curvature has become smaller. It also changes the membrane forces. Inwards buckles have extra compression and outward buckles have extra tension. When the load is increased the curvatures and membrane forces change further. At some location the Gaussian curvature becomes negative and the compression membrane force becomes large. At this location a local buckle starts. It has a larger length than the earlier buckling mode. This local buckle grows quickly, other buckles occur next to it and this spreads through the shell in a second. The shell collapses.

In other words, the shell buckling formulas do not work because the real local curvature and the real local membrane force are very different than computed by a linear elastic analysis of a perfect structure.

Measuring shape imperfections

The accurate shape of a shell structure can be measured by a laser scanner. The result is a point cloud that can be visualised by a CAD program (fig. 192). There is a simple way to extract shape imperfections from a point cloud. Load the point cloud in software Rhinoceros and fit a [NURBS](#) (p. 9) through the cloud. Choose the distance of the control points equal to

the buckling length. This fit will not follow the shape imperfections because the control points are too far apart. The software can compute the distance between a point and the NURBS. The software does this for all points in the cloud and gives a histogram of these distances (fig. 193). The largest distance is the imperfection amplitude d .

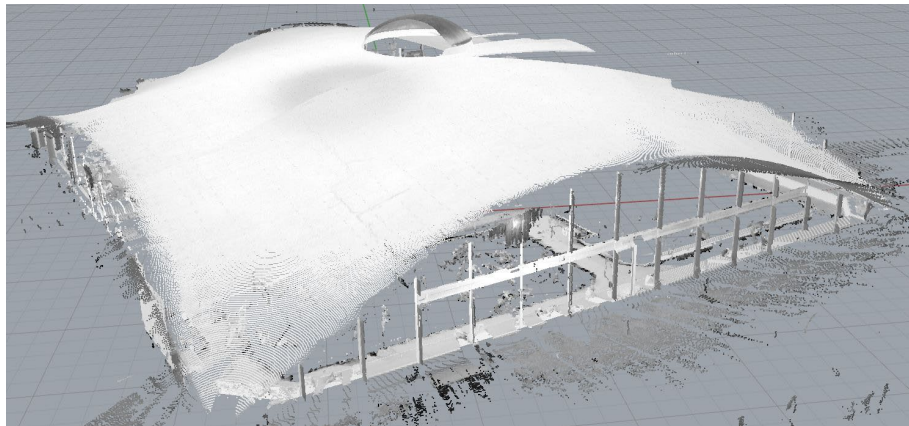


Figure 192. Point cloud of a swimming pool in Heimberg, Switzerland. The laser scanner was positioned inside. All points that are not on the shell were removed later by hand, for example walls, light fittings, swimming children [95].

Bart Elferink and Peter Eigenraam (student and teacher at Delf University) scanned four reinforced concrete shell roofs that were built by the team of Heinz Isler around 1970. The result is

$$d = \frac{1}{108} A^{0.3} l^{0.4}$$

where d is the imperfection amplitude (5% characteristic value), A is the surface area of the shell and l is the imperfection length. The partial safety factor is 1.4 [95].

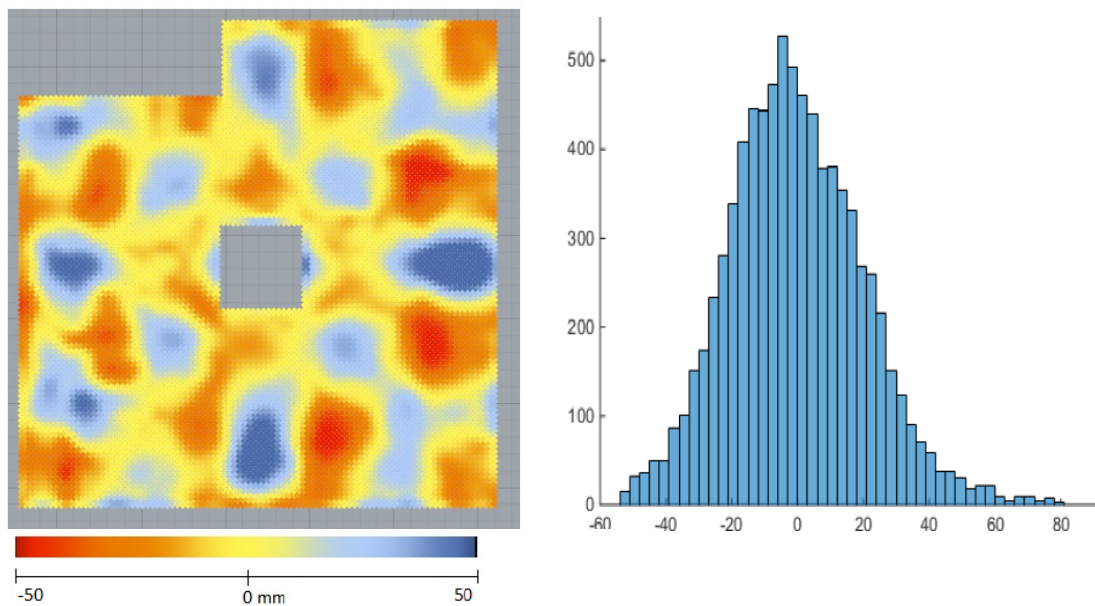


Figure 193. Shape imperfections in the shell roof of Heimberg swimming pool [95]

Stiffeners

If a shell would buckle it is technically better to use some of the shell material to design stiffeners (fig. 194).

The argument that proves this statement is simple. By putting material in another position the cross-section area stays the same. Therefore, membrane stiffness does not change and the membrane forces do not change. The bending moments in thin shells are small anyway. Consequently, the stresses do not change and it does not affect the strength of the cross-section (yielding or crushing). The material change does increase the moment of inertia, the bending stiffness and the buckling load. Q.E.D.

Of course, “technically better” can be overruled by “expensive to build”, “difficult to clean”, “just ugly” et cetera.

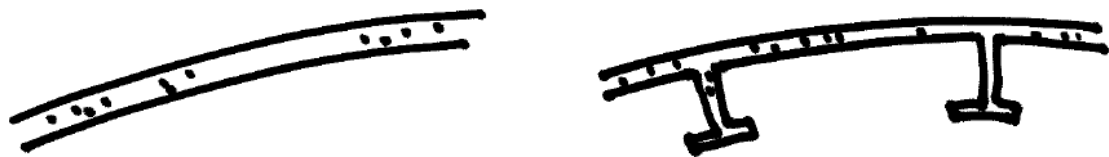


Figure 194. Cross-sections of two shell parts; left without stiffeners and right with stiffeners. Note that the cross-section areas are the same while the moments of inertia are different.

Exercise: Have you noticed that small animals like spiders have an exoskeleton and large animals like elephants have a skeleton? At what size does the transition occur? You can study this by considering a drop of water enclosed by a spherical shell. The water is loaded by gravity and the shell is supported in a point. What is the largest membrane force in the shell? What thickness is required for strength? Subsequently, enlarge the diameter until the shell buckles. At this diameter the designer needs to consider stiffeners or replace the shell by a space truss. I look forward to hearing what diameter you found.⁷



CNIT

The world largest shell structure is in Paris (fig. 196). I was built in 1956 to 1958 as an exhibition centre for machines. It is called “centre des nouvelles industries et technologies” (CNIT). Nowadays, the shell covers shops, restaurants, offices, a convention centre, a hotel and a subway station (fig. 197). Despite its size the shell is easily overlooked due to the eye catching Grande Arche, which was built next to it in 1985 to 1989. To go there take any public transportation to La Défense Grande Arche.

Architects:	Robert Camelot, Jean de Mailly and Bernard Zehrfuss
Engineers:	Nicolas Esquillan (shell) and Jean Prouvé (façade)
Consultant:	Pier Luigi Nervi
Contractors:	Balancy et Schuhl, Boussiron, Coignet
Construction time:	2.5 years
Structure:	Two layers of reinforced concrete, spaced 2 m, connected by reinforced concrete walls
Shell material:	6070 m ³ of reinforced concrete

⁷ An incomplete solution to this problem is $2a \sim \frac{f^3 \sqrt{1-\nu^2}}{\rho g E^2}$, where $2a$ is the transition diameter,

symbol \sim is read as “is proportional to”, f is the material strength, ν is Poisson’s ratio, ρ is the specific mass of water, g is the gravitational acceleration and E is Young’s modulus.

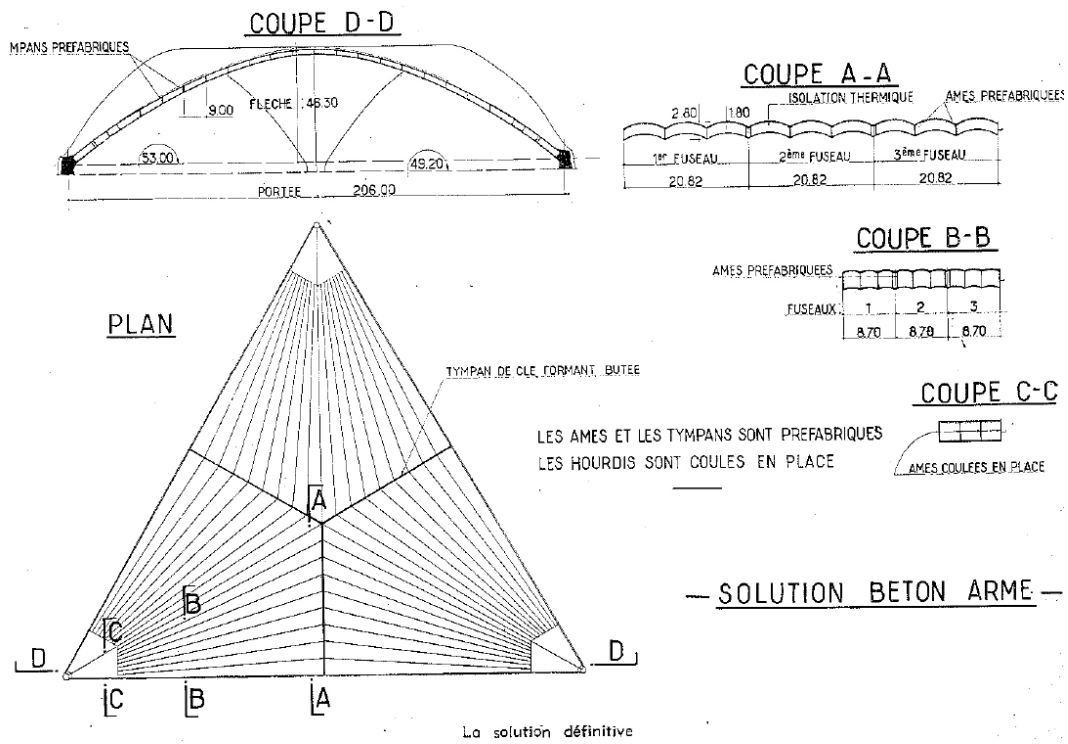


Figure 195. CNIT design by Esquillan [96]



Figure 196. CNIT in 1960 [97]



Figure 197. CNIT interior in 2010 [98]

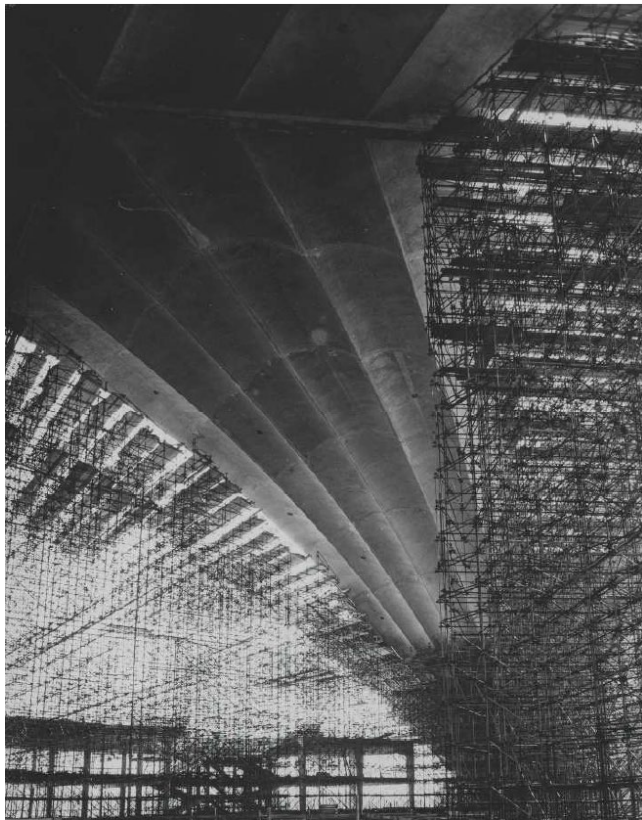


Figure 198. CNIT scaffolding [99]

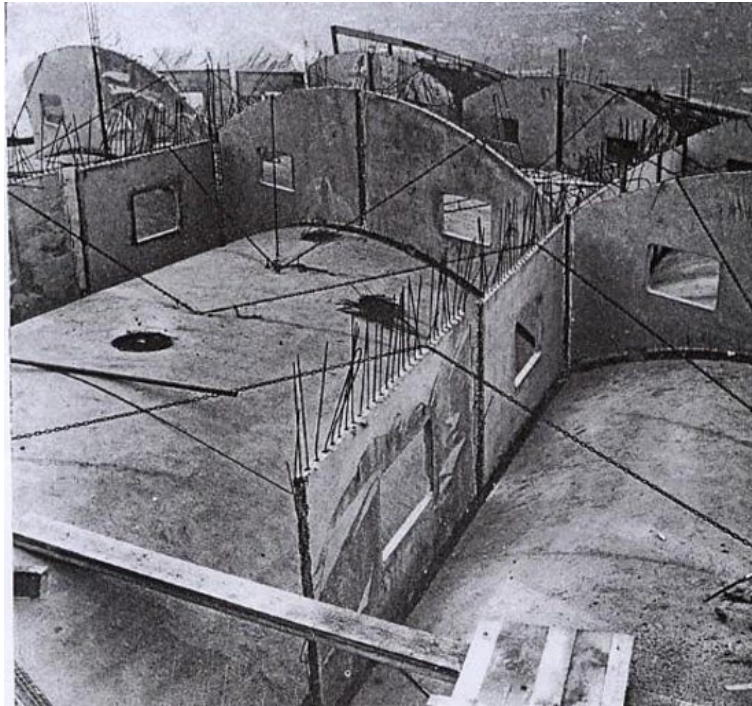


Figure 199. CNIT during construction, visible are the bottom shell and the prefab walls [100]

Each corner of the shell is supported by a large reinforced concrete block that distributes the load over the lime stone underground. The three blocks are connected to each other by three prestressed tension rods [101].

Buckling, yielding or crushing?

In steel columns there is interaction between buckling and yielding. This is mostly caused by rolling stresses and welding stresses. In this note, the theory is summarised and extended to shells.

Relative slenderness is defined as

$$\beta = \sqrt{\frac{n_p}{C n_{cr}}} = \sqrt{\frac{-f t}{C \frac{-0.6 E t^2}{a}}} = \sqrt{\frac{1}{0.6 C} \frac{f a}{E t}}$$

If $\beta \gg 1$ then buckling occurs before yielding or crushing.

If $\beta \ll 1$ then plastic failure or crushing occurs before buckling.

If $\beta \approx 1$ then interaction occurs between buckling and yielding or crushing.

Table 18 shows that a shell made of plastic is more likely to buckle than the same shell made of glass. Figure 200 shows buckling curves for steel columns based on hundreds of experiments [102]. The curves can be adopted for shell structures too, however, there is no experimental conformation.

Table 18. Properties of materials

Material	Young's modulus E	Compressive strength f	$\frac{E}{f}$
Glass	70000 N/mm ²	50 N/mm ²	1400
Concrete	35000	40	875
Aluminium	70000	110	636
Steel	210000	350	600
Wood (Pine)	13000	40	325
Plastic (Acrylic)	2300	70	33

```

> Phi:=0.5*(1+alpha*(l-0.2)+l^2):
> G:=1/(Phi+sqrt(Phi^2-l^2)):
> alpha:=0.13: f1:=simplify(G): # a0
> alpha:=0.21: f2:=simplify(G): # a
> alpha:=0.34: f3:=simplify(G): # b
> alpha:=0.49: f4:=simplify(G): # c
> alpha:=0.76: f5:=simplify(G): # d
> plot({f1,f2,f3,f4,f5, 1/l^2},l=0..3,0..1);

```

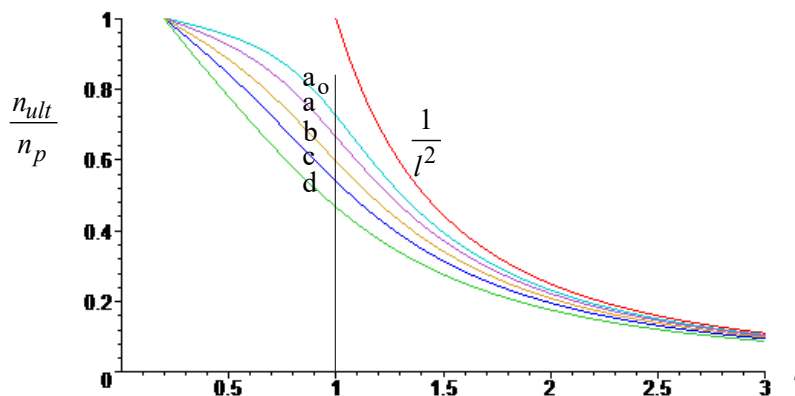


Figure 200. Eurocode buckling curves for steel columns

Exercise: What percentage of shells fails due to buckling and not due to yielding or crushing?

Assume uniform distributions of the material properties $33 \leq \frac{E}{f} \leq 1400$, geometry $30 \leq \frac{a}{t}$

≤ 1000 and knock down factor $\frac{1}{6} \leq C \leq 1$. (The exact answer is $\frac{102499-90(\ln 2+\ln 3)}{132599} 100\%$.)

Buckling curves for computational analysis

When a steel cross-section has residual stresses and it is loaded in compression than local yielding can occur. This reduces the bending stiffness. Residual stresses can be included in finite element models, however, this takes much modelling time and computation time. There is a much easier way to include the effect of residual stresses in a finite element analysis.

Rewrite the eurocode buckling curves (fig. 200) and implement a reduction factor $\frac{n_{ult}}{C n_{cr}}$ on

the bending stiffness as a function of the normal force $\frac{n}{n_p}$ (fig. 201) [103]. The derivation

below has been performed by Maple.

```

> Phi:=0.5*(1+alpha*(l-0.2)+l^2):
> G1:=1/l^2:
> G2:=1/(Phi+sqrt(Phi^2-l^2)): # ECCS buckling curve
> opl:=solve(G=G2,l): l:=opl[2]:

```

```

> alpha:=0.13: f1:=simplify(G2/G1): # a0
> alpha:=0.21: f2:=simplify(G2/G1): # a
> alpha:=0.34: f3:=simplify(G2/G1): # b
> alpha:=0.49: f4:=simplify(G2/G1): # c
> alpha:=0.76: f5:=simplify(G2/G1): # d
> plot({f1,f2,f3,f4,f5},G=0..1);

```

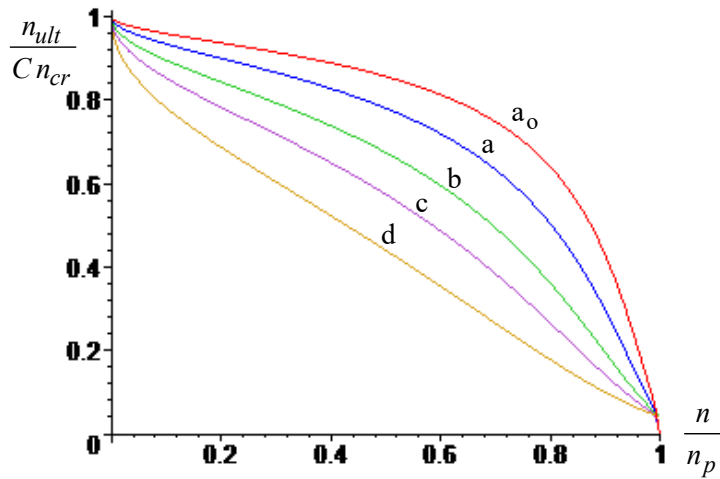


Figure 201. Reduction factor of the initial bending stiffness as a function of the normal force

The tangent bending stiffness in the presence of a bending moment is also significantly influenced by rolling and welding stresses (fig. 202). This can be included in the moment-curvature diagram.

Figure 202. Moment curvature diagram of a rectangular steel cross-section. Shown are the influence of normal force and residual stresses [104].

Literature

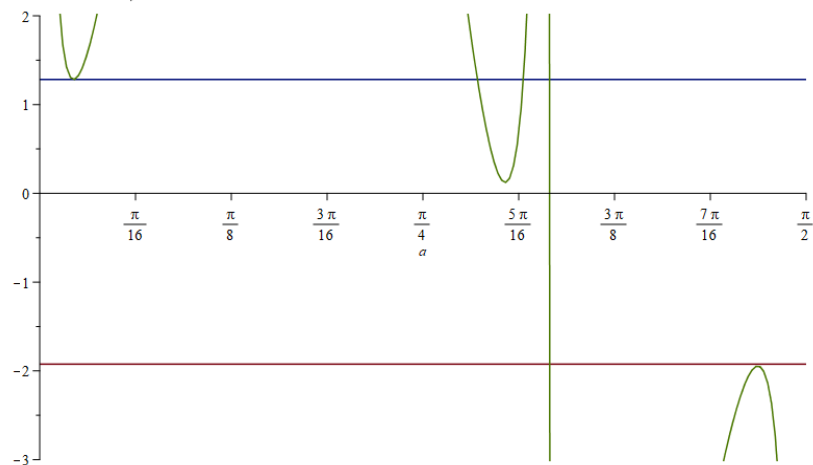
81. M. Ketchum, "Memoirs of Milo Ketchum", <http://www.ketchum.org/-milo/index.html>
82. P.K. Malhotra, T. Wenk, M. Wieland, "Simple Procedure for Seismic Analysis of Liquid-Storage Tanks", *Structural Engineering International*, 2000, No. 3, pp. 197-210.
83. Y. Yoshimura, "On the Mechanism of Buckling of a Circular Shell under Axial Compression", NACA Technical memorandum No. 1390, Sec 7.7, 1955.
84. N.J. Hoff, The perplexing behaviour of thin circular cylindrical shells in axial compression, report SUUDAR No. 256, Stanford University 1966.
85. A. Robertson, The strength of tubular struts, proceedings of the Royal Society A, Mathematical, physical and engineering sciences, Vol. 121, Issue 788, Dec. 1928
86. V.I. Weingarten, E.J. Morgan, P. Seide, "Elastic Stability of Thin-Walled Cylindrical and Conical Shells under combined Internal Pressure and Axial Compression", *AIAA Journal*, Vol. 3, 1965, pp. 500-505.
87. Th. von Kármán, L.G. Dunn, H.S. Tsien, "The influence of Curvature on the Buckling Characteristics of Structures", *J. Aero. Sci.*, 7(7) , 1940, pp. 276-89 (Sec. 7.7).
88. W.T. Koiter, "Over de Stabiliteit van het Elastisch Evenwicht", Publisher H.J. Paris, Amsterdam, 1945 (In Dutch).
89. W.T. Koiter, NASA Technical Translation F10,833, 1967.
90. M. Farshad, "Design and Analysis of Shell Structures", Kluwer Academic Publishers, Dordrecht, 1992.
91. J. Arbocz, "Shell Buckling Research at Delft 1976-1996", Report TU Delft, 1996.
93. L.A. Samuelson, S. Eggwertz, "Shell Stability Handbook", Elsevier Science Publishers LTD, Essex, 1992.
94. I. Elishakov. Resolution of the twentieth century conundrum in elastic stability. Florida Atlantic University, USA, 2014.
95. B. Elferink, P. Eigenraam, P.C.J. Hoogenboom, J.G. Rots, Shape imperfections of reinforced concrete shell roofs, *Heron*, Vol. 61 (2016) No. 3, pp. 177-192.
96. CNIT, ...
97. CNIT, ...
98. CNIT, ...
99. CNIT, ...
100. CNIT, ...
101. Michel Pré, The CNIT–La Défense Railway Station in Paris: Answers to Complex Constraints, *Structural Engineering International*, Vol. 28, 2018, Issue 2, Pages 157-160 , Published online: <https://www.tandfonline.com/doi/full/10.1080/10168664.2018.1450698>
102. ...
103. Xia Wenjing, P.C.J. Hoogenboom, "Buckling analysis of offshore jackets in removal operations", Proceedings of OMAE conference, June 19-24 2011, Rotterdam
104. J. Witteveen, reader, ...

Appendix 10

```

> nxy := 0 : nyx := 0 : kxy := 0 :
> uz := C · cos( Pi · x / lx ) · cos( Pi · y / ly ) :
> G1 := kxx · diff(uz, y, y) - 2 · kxy · diff(uz, x, y) + kyy · diff(uz, x, x) :
> G2 := kxx · diff(G1, y, y) - 2 · kxy · diff(G1, x, y) + kyy · diff(G1, x, x) :
> D1 := diff(uz, x, x) + diff(uz, y, y) :
> D2 := diff(D1, x, x) + diff(D1, y, y) :
> D3 := diff(D2, x, x) + diff(D2, y, y) :
> D4 := diff(D3, x, x) + diff(D3, y, y) :
> P1 := lambda · (pz + nxx · diff(uz, x, x) + (nxy + nyx) · diff(uz, x, y) + myy · diff(uz, y, y)) :
> P2 := diff(P1, x, x) + diff(P1, y, y) :
> P3 := diff(P2, x, x) + diff(P2, y, y) :
> eq := (E · t^3 / (12 · (1 - v^2))) · D4 + E · t · G2 = P3 :
> lambda := solve(eq, lambda) :
> lambda2 := (-E · t / (nxx / lx^2 + myy / ly^2)) · ( (pi^2 · t^2 / (12 · (1 - v^2))) · (1 / lx^2 + 1 / ly^2)^2 + ( (kxx / ly^2 + kyy / lx^2)^2 + (2 · kxy / (lx · ly))^2 ) / (pi^2 · (1 / lx^2 + 1 / ly^2)^2) ) :
> simplify(lambda - lambda2);
0
> lx := l · cos(a) : ly := l · sin(a) :
> lambda3 := simplify(lambda2) :
> lambda4 := (-E · t^2 / (sqrt(3 · (1 - v^2)))) · (abs(kxx) / myy) :
> lambda5 := (-E · t^2 / (sqrt(3 · (1 - v^2)))) · (abs(kyy) / nxx) :
> E := 5 : nu := 0.3 : t := 3 : l := 1 / abs(kyy) :
> kxx := 1 / 150 · (1 / (t · sqrt(1 - v^2))) : kyy := -1 / 300 · (1 / (t · sqrt(1 - v^2))) : nxx := 1 / 1000 · (E · t / (1 - v^2)) : myy := -3 / 1000 · (E · t / (1 - v^2)) :
> nxx · abs(kxx) + myy · abs(kyy);
-0.00001919935600
> plot( { lambda3, lambda4, lambda5 }, a = 0 .. Pi / 2, -3 .. 2);

```



Appendix 20

Equations for imperfection sensitivity

This note proposes a simple model for imperfection sensitivity. Consider a shell with an invisible imperfection in the shape of a ring buckling pattern (fig. 13). To keep the model simple, $k_{xy} = 0$ and $n_{xy} = n_{yx} = 0$. The amplitude of the imperfection is d and its length is l_{cr} .

$$l_{cr} = \frac{\pi}{\sqrt[4]{12(1-\nu^2)}} \sqrt{\frac{t}{|k_{yy}|}} \dots\dots\dots \text{buckling length (p. 139)} \dots\dots\dots (1)$$

We compare the meridional (p. 14) curvature k_{xx} of the perfect undeformed shell to the meridional local curvature k'_{xx} of the imperfect deformed shell. The shell load n_{xx} increases the imperfection d by an amplitude w (fig. 13). In an inward buckle the curvature is

$$k'_{xx} = k_{xx} - \pi^2 \frac{d+w}{l_{cr}^2} \dots\dots\dots \text{surface curvature (p. 19, appendix 20)} \dots (2)$$

The shell can be seen as a stack of hoops. A hoop that has become larger has an additional tension membrane force. A hoop that has become smaller has an additional compression membrane force.

$$\varepsilon_{yy} = -wk_{yy} \dots\dots\dots \text{membrane equation 8 (p. 36)} \dots\dots\dots (3)$$

$$n'_{yy} = n_{yy} + Et\varepsilon_{yy} \dots\dots\dots \text{membrane equation 5 (p. 36)} \dots\dots\dots (4)$$

where n_{yy} is the force in the perfect hoop and n'_{yy} is the force in the imperfect and deformed hoop. The material in the latter hoop is compressed in two directions, by n_{xx} and by n'_{yy} (fig. 14). This is the location where the shell will buckle. The buckle is resisted by bending deformation too. A plate deformed in a sinusoidal deformation will resist with a stress p .

$$p = \frac{Et^3}{12(1-\nu^2)} \frac{\pi^4 w}{l_{cr}^4} \dots\dots\dots \text{appendix 20 (p.)} \dots\dots\dots (5)$$

The surface load p_z is the same on the perfect shell and on the imperfect deformed shell.

So $p_z = p'_z$ or

$$n_{xx}k_{xx} + n_{yy}k_{yy} = n_{xx}k'_{xx} + n'_{yy}k_{yy} - p \dots\dots\dots \text{membrane equation 1 (p. 36)} \dots\dots\dots (6)$$

The additionally compressed hoop has a negative Gaussian curvature. It will buckle as a flat plate. The buckling length is $2l_{cr}$ (fig. 13). This is the centre-to-centre distance of the additionally tensioned rings. However, the additional hoop force is not uniform but sinusoidal. Therefore, a buckling length of $\sqrt{2} l_{cr}$ is proposed. This buckling length produces a knock down factor of exactly 1/6 when d goes to infinity.

$$l_x = \sqrt{2} l_{cr} \dots\dots\dots (7)$$

$$\frac{k'_{xx}}{l_y^2} + \frac{k_{yy}}{l_x^2} = 0 \dots\dots\dots \text{buckling mode 3 (p. 141)} \dots\dots\dots (8)$$

$$\frac{n_{xx}}{l_x^2} + \frac{n'_{yy}}{l_y^2} = \frac{-\pi^2 Et^3}{12(1-\nu^2)} \left(\frac{1}{l_x^2} + \frac{1}{l_y^2}\right)^2 \dots\dots\dots \text{buckling mode 3 (p. 141)} \dots\dots\dots (9)$$

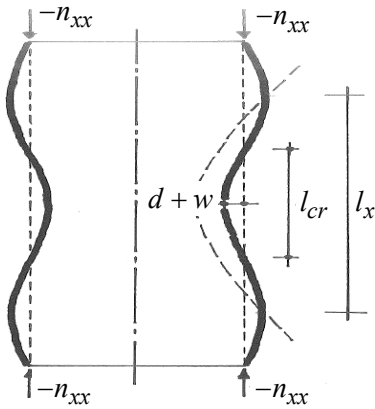


Figure 13. Longitudinal section of the shell

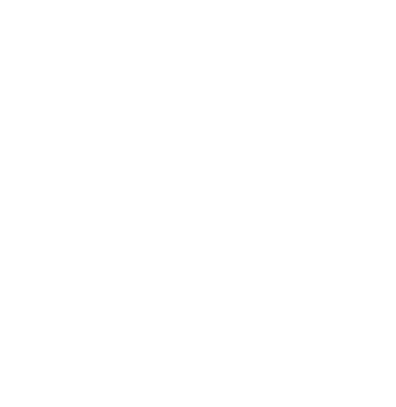


Figure 14. Membrane forces in a compressed ring part

The membrane force n_{xx} that satisfies equations 1 to 9 is the ultimate load (appendix 20). It can be solved iteratively from the following three equations. The iterations converge quickly for $d > \frac{1}{2}t$ approximately. (Convergeert ook niet als n_{yy}/n_{xx} negatief.)

$$\lambda_{ult1} = \frac{-Et^2}{\sqrt{3(1-\nu^2)}} \frac{|k_{yy}|}{n_{xx}} C \quad C = \frac{\left(\frac{k_{xx}}{k_{yy}} - 1 - 2\eta \frac{d}{t}\right)^2}{4 \left(\frac{k_{xx}}{k_{yy}} - \frac{n_{yy}}{n_{xx}} - 3\eta \frac{d}{t}\right) \left(\frac{k_{xx}}{k_{yy}} - 2\eta \frac{d}{t}\right)} \quad \eta = \frac{\sqrt{3(1-\nu^2)}}{1-C}$$

Exercise: The above equation gives the knockdown factor C (p. 144) of buckling mode 1 (p. 140). What needs to be changed to the equations to compute the knockdown factor of buckling mode 2?

Exercise: What is the limit of C for d to infinity?

Challenge: Find equations that do converge for $d < \frac{1}{2}t$.

Demonstration of the imperfection sensitivity model

Consider an axially loaded cylinder $E = 2.1 \cdot 10^5 \text{ N/mm}^2$, $\nu = 0.35$, $a = 200 \text{ mm}$, $t = 1 \text{ mm}$, $d = \frac{1}{2}t$. The equations for imperfection sensitivity (p. 146) are used to compute the response for increasing load. Figure 15 shows that the local curvature k'_{xx} in the meridional direction is significant. This cannot be observed by the naked eye. It is caused by the imperfection d which grows during loading by w .

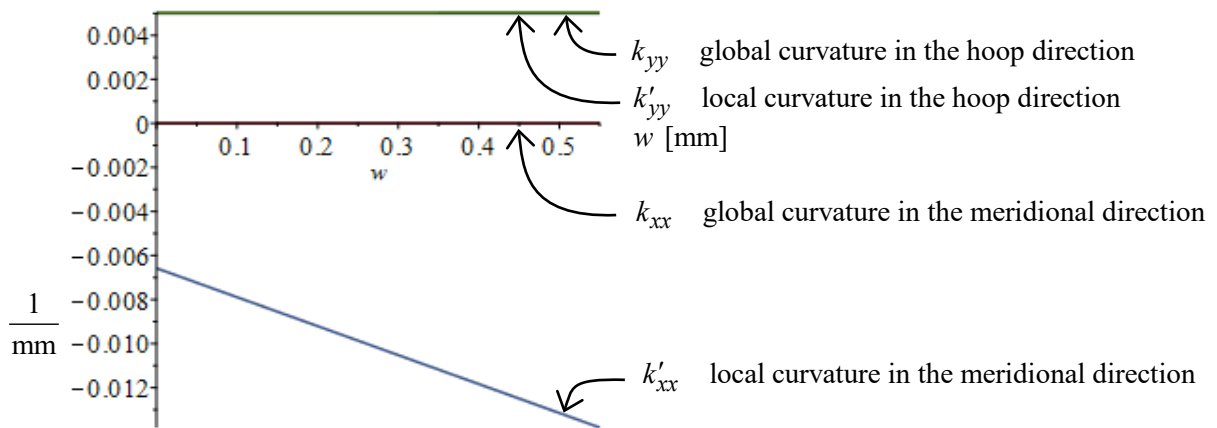


Figure 15. Curvatures at the buckling location as a function of the deformation w

Figure 16 shows that the local membrane force n'_{yy} in the hoop direction is significant. This is also due to the shape imperfection d . The imperfections are invisible but have large consequences. Figure 17 shows that this model predicts a reduction in buckling load that is even more dramatic than Koiter's law (p. ...).

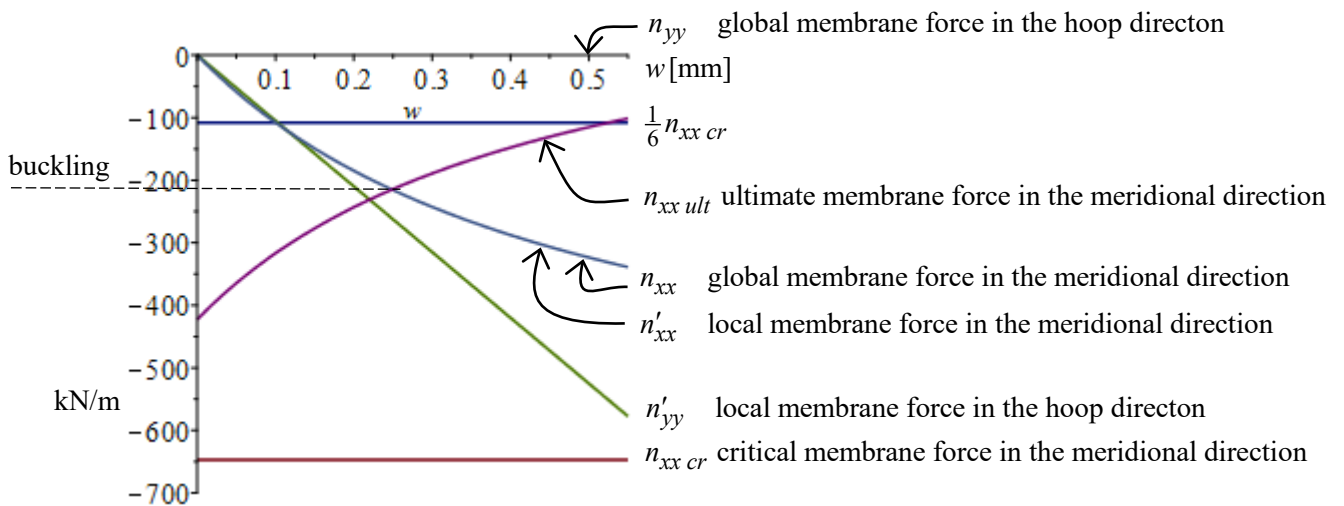


Figure 16. Membrane forces at the buckling location as a function of the deformation w

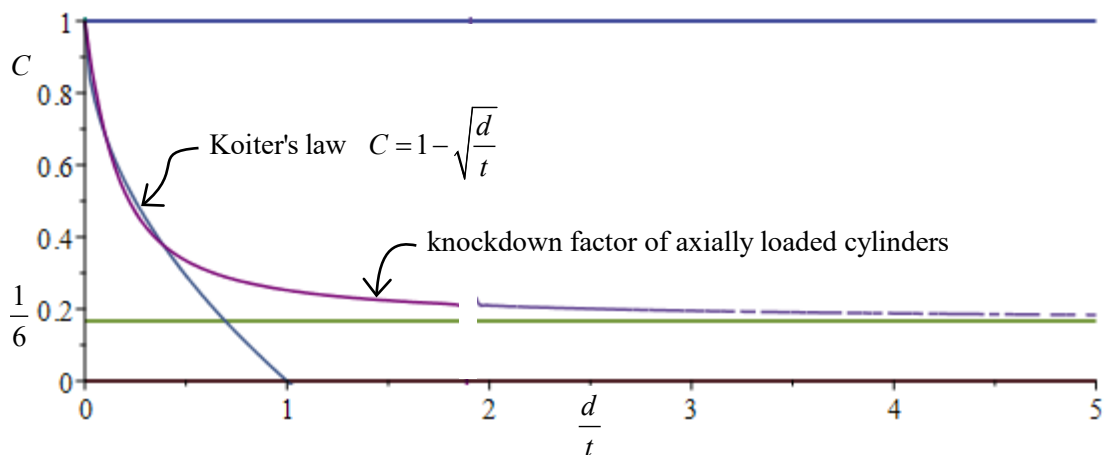


Figure 17. Knockdown factor C as a function of the imperfection amplitude d

Exercise: The formulas (p. 147) show that the knockdown factor of an axially loaded cylinder ($k_{xx} = n_{yy} = 0$) depends on its d/t ratio only. Compare figure 17 to figure 9. What is the relation between imperfection d and radius a ? Does this make sense?

$$\begin{aligned}
 > lcr := \frac{\pi}{(12 \cdot (1 - \nu^2))^{\frac{1}{4}}} \cdot \text{sqrt}\left(\frac{t}{k_{yy}}\right); \\
 > k_{xxl} := k_{xx} - \frac{\text{Pi}^2 \cdot (d + w)}{lcr^2}; \\
 > e_{yy} := -w \cdot k_{yy}; \\
 > n_{yy} := n_{yy} + E \cdot t \cdot e_{yy}; \\
 > eq1 := n_{xx} \cdot k_{xx} + n_{yy} \cdot k_{yy} + 0 = n_{xx} \cdot k_{xxl} + n_{yy} \cdot k_{yy} - \frac{E \cdot t^3}{12 \cdot (1 - \nu^2)} \cdot \frac{\text{Pi}^4 \cdot w}{lcr^4}; \\
 > l_x := \text{sqrt}(2) \cdot lcr; \\
 > l_y := l_x \cdot \text{sqrt}\left(-\frac{k_{xxl}}{k_{yy}}\right); \\
 > eq2 := \frac{n_{xx}}{l_x^2} + \frac{n_{yy}}{l_y^2} = \frac{-\pi^2 \cdot E \cdot t^3}{12 \cdot (1 - \nu^2)} \cdot \left(\frac{1}{l_x^2} + \frac{1}{l_y^2}\right)^2; \\
 > \# ----- solution to the equations ----- \\
 > n_{xx} := \frac{-E \cdot t^2}{\sqrt{3 \cdot (1 - \nu^2)}} \cdot k_{yy} \cdot C; \\
 > w1 := \text{solve}(eq1, w); \\
 > w2 := d \cdot \frac{C}{1 - C}; \\
 > \text{simplify}(w1 - w2); \\
 & \hspace{15em} 0 \\
 > \# \text{ definition } \eta := \frac{d}{t} \cdot \frac{\sqrt{3 \cdot (1 - \nu^2)}}{1 - C}; \\
 > k_{xx} := \alpha \cdot k_{yy}; \quad n_{yy} := \beta \cdot n_{xx}; \quad w := d \cdot \frac{C}{1 - C}; \quad d := \eta \cdot t \cdot \frac{1 - C}{\sqrt{3 \cdot (1 - \nu^2)}}; \\
 > C := \text{simplify}(\text{solve}(eq2, C)); \\
 & \hspace{15em} C := \frac{(-2\eta + \alpha - 1)^2}{4(\alpha - \beta - 3\eta)(\alpha - 2\eta)} \\
 > \frac{(-2)^2}{4 \cdot (-2) \cdot (-3)}; \\
 & \hspace{15em} \frac{1}{6}
 \end{aligned}$$

> restart : # ----- beam with a cosin load -----

> $q := qt \cdot \cos\left(\frac{\text{Pi} \cdot x}{l}\right) :$

> $w := wt \cdot \cos\left(\frac{\text{Pi} \cdot x}{l}\right) :$

> $eq := q = EI \cdot \text{diff}(w, x, x, x, x) :$

> $qt := \text{solve}(eq, qt) :$

$$qt := \frac{EI \pi^4 wt}{l^4}$$

> restart : # ----- curvature of an inward imperfection -----

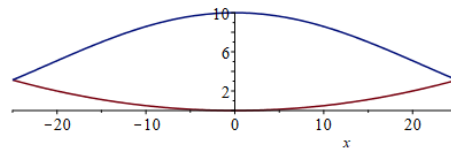
> $z1 := \frac{1}{2} \cdot kxx \cdot x^2 :$

> $z2 := (d + w) \cdot \cos\left(\frac{\text{Pi} \cdot x}{l}\right) :$

> $z := z1 + z2 :$

> $t := 1 : kxx := \frac{1}{100 \cdot t} : d := 5 \cdot t : w := 5 \cdot t : l := \frac{1}{2 \cdot kxx} :$

> $\text{plot}\left(\{z1, z\}, x = -\frac{l}{2} .. \frac{l}{2}\right) :$



> $t := 't' : kxx := 'kxx' : d := 'd' : w := 'w' : l := 'l' :$

> $kxxl := \text{diff}(z, x, x) :$

> $x := 0 : kxxl := \text{simplify}(kxxl) :$

$$kxxl := kxx - \frac{(d + w) \pi^2}{l^2}$$

Appendix 21

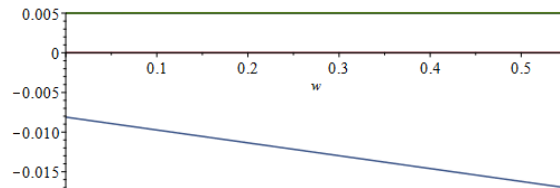
> $E := 2.1e5$: $\nu := 0.35$: $a := 200 \cdot t$: $t := 1$: $d := \frac{1}{2} \cdot t$: $k_{yy} := \frac{1}{a}$: $k_{xx} := 0$: $m_{yy} := 0$: $n_{xx} :$

> $lcr := \frac{\text{Pi}}{(12 \cdot (1 - \nu^2))^{\frac{1}{4}}} \text{sqrt}\left(\frac{t}{k_{yy}}\right) :$

> $k_{xxl} := k_{xx} - \text{Pi}^2 \cdot \frac{d + w}{lcr^2} :$

> $k_{yyt} := \frac{1}{a - d - w} :$

> $\text{plot}(\{k_{xx}, k_{xxl}, k_{yy}, k_{yyt}\}, w = 0 .. 0.55 \cdot t) ;$



> $e_{yy} := -w \cdot k_{yy} :$

> $m_{yyl} := m_{yy} + E \cdot t \cdot e_{yy} :$

> $eq1 := n_{xx} \cdot k_{xx} + m_{yy} \cdot k_{yy} + 0 = n_{xx} \cdot k_{xxl} + m_{yyl} \cdot k_{yy} - \frac{E \cdot t^3}{12 \cdot (1 - \nu^2)} \cdot \frac{\text{Pi}^4 \cdot w}{lcr^4} :$

> $n_{xx} := \text{solve}(eq1, n_{xx}) :$

> $l_x := \text{sqrt}(2) \cdot lcr :$

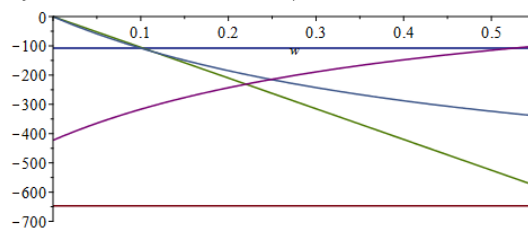
> $l_y := l_x \cdot \text{sqrt}\left(-\frac{k_{xxl}}{k_{yy}}\right) :$

> $n_{xx_ult} := l_x^2 \cdot \left(\frac{-\text{Pi}^2 \cdot E \cdot t^3}{12 \cdot (1 - \nu^2)} \left(\frac{1}{l_x^2} + \frac{1}{l_y^2} \right)^2 - \frac{m_{yyl}}{l_y^2} \right) :$

> $n_{xxl} := n_{xx} \cdot \frac{2 \cdot \text{Pi} \cdot a}{2 \cdot \text{Pi} \cdot (a - d - w)} :$

> $n_{xx_cr} := \frac{-E \cdot t^2 \cdot k_{yy}}{\text{sqrt}(3 \cdot (1 - \nu^2))} :$

> $\text{plot}\left(\left\{n_{xx}, n_{xx_ult}, m_{yyl}, n_{xx_cr}, \frac{n_{xx_cr}}{6}\right\}, w = 0 .. 0.55 \cdot t, -700 .. 0\right) ;$



$$> \eta := \frac{\text{sqrt}(3 \cdot (1 - \nu^2))}{1 - C} :$$

$$> eq := C = \frac{\left(\frac{k_{xx}}{k_{yy}} - 1 - 2 \cdot \eta \cdot \frac{d}{t}\right)^2}{4 \cdot \left(\frac{k_{xx}}{k_{yy}} - \frac{m_{yy}}{n_{xx}} - 3 \cdot \eta \cdot \frac{d}{t}\right) \cdot \left(\frac{k_{xx}}{k_{yy}} - 2 \cdot \eta \cdot \frac{d}{t}\right)} :$$

> opl := solve(eq, C) : # 3 solutions

> E := 2.1e5 : nu := 0.35 : a := 200 · t : t := 1 : kyy := $\frac{1}{a}$: kxx := 0.1 · kyy : nxx := -100 : nyy := 0.01 · nxx :

> plot($\left\{0, \frac{1}{6}, 1, \text{opl}[1], \text{opl}[2], \text{opl}[3], 1 - \text{sqrt}(d)\right\}, d=0..5, 0..1$);

